

12
03

LEVEL #

AD-E 300 889 #

DNA 5274T

AD A088916

SPHERICALLY SYMMETRIC CALCULATIONS OF THE SRI GROUT SPHERES EXPERIMENT FOR FOUR DIFFERENT LABORATORY CONFIGURATIONS

Systems, Science and Software
P.O. Box 1620
La Jolla, California 92038

31 March 1980

Topical Report for Period 1 January 1979—31 March 1980

CONTRACT No. DNA 001-79-C-0099

APPROVED FOR PUBLIC RELEASE;
DISTRIBUTION UNLIMITED.

THIS WORK SPONSORED BY THE DEFENSE NUCLEAR AGENCY
UNDER RDT&E RMSS CODE B345079462 J24AAXYX98366 H2590D.

DDC FILE COPY

Prepared for
Director
DEFENSE NUCLEAR AGENCY
Washington, D. C. 20305

DTIC
ELECTE
S SEP 8 1980 D
B

80 8 18 053

Destroy this report when it is no longer
needed. Do not return to sender.

PLEASE NOTIFY THE DEFENSE NUCLEAR AGENCY,
ATTN: STTI, WASHINGTON, D.C. 20305, IF
YOUR ADDRESS IS INCORRECT, IF YOU WISH TO
BE DELETED FROM THE DISTRIBUTION LIST, OR
IF THE ADDRESSEE IS NO LONGER EMPLOYED BY
YOUR ORGANIZATION.



18 DNA, SBIE /

UNCLASSIFIED

SECURITY CLASSIFICATION OF THIS PAGE (When Data Entered)

19 REPORT DOCUMENTATION PAGE		READ INSTRUCTIONS BEFORE COMPLETING FORM
1. REPORT NUMBER DNA 5274T, AD-E300 889 / AD-A088916	2. GOVT ACCESSION NO.	3. RECIPIENT'S CATALOG NUMBER 9
4. TITLE (and Subtitle) SPHERICALLY SYMMETRIC CALCULATIONS OF THE SRI GROUT SPHERES EXPERIMENT FOR FOUR DIFFERENT LABORATORY CONFIGURATIONS.		5. DATE OF REPORT PERIOD COVERED Topical Report, for period 1 Jan 79-31 Mar 80
7. AUTHOR(s) Norton/Rimer K./Lie	14 X983	6. PERFORMING ORG. REPORT NUMBER SSS-R-80-4240
9. PERFORMING ORGANIZATION NAME AND ADDRESS Systems, Science and Software P.O. Box 1620 La Jolla, California 92038	15	8. CONTRACT OR GRANT NUMBER(s) DNA 001-79-C-0099
11. CONTROLLING OFFICE NAME AND ADDRESS Director Defense Nuclear Agency Washington, D.C. 20305	11	10. PROGRAM ELEMENT, PROJECT, TASK AREA & WORK UNIT NUMBERS Subtask J24AAXY 983-66
14. MONITORING AGENCY NAME & ADDRESS (if different from Controlling Office) 12 50		12. REPORT DATE 31 March 1980
		13. NUMBER OF PAGES 50
		15. SECURITY CLASS (of this report) UNCLASSIFIED
		15a. DECLASSIFICATION/DOWNGRADING SCHEDULE
16. DISTRIBUTION STATEMENT (of this Report) Approved for public release; distribution unlimited.		
17. DISTRIBUTION STATEMENT (of the abstract entered in Block 20, if different from Report)		
18. SUPPLEMENTARY NOTES This work sponsored by the Defense Nuclear Agency under RDT&E RMSS Code B345079462 J24AAXYX98366 H2590D.		
19. KEY WORDS (Continue on reverse side if necessary and identify by block number) Grout Spheres Shock Waves Finite Difference Calculations Hydrofracture		
20. ABSTRACT (Continue on reverse side if necessary and identify by block number) One-dimensional spherically symmetric finite difference calculations are presented which attempt to simulate the Stanford Research Institute (SRI) Containment experiments. In these experiments, 3/8 gm spherical PETN charges are detonated in 12-inch diameter spheres of grout placed in a water tank forming a cavity from which, subsequently, the spheres are hydrofractured using water or glycerol. The finite difference calculations simulate the formation of compressive residual stress fields around the explosively		

388507 DW

UNCLASSIFIED

SECURITY CLASSIFICATION OF THIS PAGE(When Data Entered)

20. ABSTRACT (Continued)

M/CR^o

generated cavities. These calculations were made for three types of grout; SRI rock matching grout (2C4), granite simulant (GS3), and a low density grout (LD2C4) which is a mixture of 2C4 grout with glass microspheres. The simulated cavity pressures at 100 μ sec are considerably greater than the average fracture initiation pressure from the laboratory tests yet are contained without fracturing by the residual stress fields calculated using laboratory strength data for grout. If the finite difference calculations are correct, the strong implication is that the compressive residual stress fields must have decayed significantly in the time interval between the dynamic calculations and the beginnings of the hydrofracture process. The finite difference calculations have been compared with the experimental data relevant to the dynamic time scale, which consist of cavity radius measurements and of pressure and impulse measurements made by a quartz gauge in the wall of the water tank. The best agreement between these data and calculations are obtained when a strain rate-dependent shear failure model is used to increase the shear strength in the grouts from the laboratory measured values. These result in still higher cavity pressures and residual stresses and less agreement with the measured fracture initiation pressures.

UNCLASSIFIED

SECURITY CLASSIFICATION OF THIS PAGE(When Data Entered)

TABLE OF CONTENTS

<u>Section</u>		<u>Page</u>
1	INTRODUCTION AND SUMMARY - - - - -	5
2	CONSTITUTIVE MODELS AND MATERIAL PROPERTIES DATA - - - -	10
	2.1 LABORATORY DATA - - - - -	10
	2.2 ROCK-MATCHING GROUT MODEL (2C4) - - - - -	12
	2.3 GRANITE SIMULANT MODEL (GS3) - - - - -	16
	2.4 LOW DENSITY ROCK MATCHING GROUT MODEL (LD2C4) - - -	20
	2.5 DYNAMIC STRENGTH MODELS - - - - -	22
3	CALCULATIONAL RESULTS - - - - -	23
	3.1 DESCRIPTION OF CALCULATIONS - - - - -	23
	3.2 COMPARISONS BETWEEN CALCULATIONS AND CAVITY RADIUS AND QUARTZ GAUGE DATA - - - - -	27
	3.3 DISCUSSION AND RESULTS - - - - -	31
4	REFERENCES - - - - -	45

ACCESSION for		
NTIS	White Section	<input checked="" type="checkbox"/>
DDC	Buff Section	<input type="checkbox"/>
UNANNOUNCED <input type="checkbox"/>		
JUSTIFICATION _____		
BY _____		
DISTRIBUTION/AVAILABILITY CODES		
Dist.	AVAIL	and/or SPECIAL
A		

LIST OF ILLUSTRATIONS

<u>Figure</u>		<u>Page</u>
1	Load-unload curves for 2C4 grout - - - - -	15
2	Old and new failure surfaces for 2C4 grout - - - - -	17
3	Specific volume load-unload curves for granite simulant (GS3) - - - - -	18
4	Failure surface for granite simulant (GS3) - - - - -	19
5	Load-unload curves for low-density rock-matching grout LD2C4 - - - - -	21
6	Comparison between quartz gauge record (Test 157, Impulse = 761 bars- μ sec) and calculations for 2C4 grout - - - - -	28
7	Comparison between quartz gauge records (Tests 201 and 202) and calculations for LD2C4 group - - - - -	30
8	Simulated quartz gauge records for granite simulant GS3 tests - - - - -	32
9	Simulated quartz gauge records for decoupled 2C4 grout tests - - - - -	33
10	Peak stress (overstress) vs range for 2C4 decoupled 2C4, LD2C4 (preliminary, final static and dynamic models) and GS3 spheres using failure data - - - - -	35
11	Residual stress fields at 99 μ sec for decoupled 2C4 calculation 2 (static failure model) - - - - -	37
12	Residual stress fields at 100 μ sec for decoupled 2C4 calculation 8 (dynamic failure model) - - - - -	38
13	Residual stress fields at 84 μ sec for 2C4 calculation 1 (static failure model) - - - - -	39
14	Residual stress fields at 79 μ sec for 2C4 calculation 7 (dynamic failure model) - - - - -	40
15	Residual stress fields at 124 μ sec for LD2C4 calculation 6 (static failure model) - - - - -	41
16	Residual stress fields at 110 μ sec for LD2C4 calculation 10 (dynamic failure model) - - - - -	42

LIST OF ILLUSTRATIONS (Continued)

<u>Figure</u>		<u>Page</u>
17	Residual stress fields at 95 μ sec for GS3 calculation 3 (static failure model) - - - - -	43
18	Residual stress fields at 74 μ sec for GS3 calculation 9 (dynamic failure model) - - - - -	44

LIST OF TABLES

<u>Table</u>		<u>Page</u>
1	Physical and mechanical properties data - - - - -	11
2	Average strengths of RMG 2C4, LD2C4, and GS - - - - -	13
3	Summary of 2C4 grout material properties data - - - - -	14
4	Dependence of failure surfaces on strain rate - - - - -	24
5	Summary of results of calculations - - - - -	25

I. INTRODUCTION AND SUMMARY

As part of the DNA stemming and containment program for underground nuclear testing, Stanford Research Institute (SRI) is conducting laboratory experiments to study the residual stress fields around explosively formed cavities. The standard experiment involves casting a 12-inch diameter sphere of rock matching grout (2C4) around a lucite-encased sphere of high explosive (PETN), placing this grout sphere in a pressurized water tank to simulate overburden pressure, and detonating the PETN. While maintaining overburden pressure, the sphere is then hydrofractured from the explosively formed cavity. A detailed description and discussion of the experimental results may be found in Cizek and Florence^(1, 2).

Systems, Science and Software (S³) was asked to numerically simulate these experiments in order to increase understanding of the laboratory results, and to validate our capability to calculate containment related phenomena. One part of our calculational effort, the numerical simulation of the high explosive detonation and the subsequent nonlinear dynamic processes which result in the formation of a compressive residual stress field in the grout surrounding the exploded cavity, has been reported by Rimer and Lie⁽³⁾. Since the major laboratory data consist of graphs of hydrofracture pressure vs. volume of fluid pumped into the cavity, the only data available to be compared to the dynamic calculations consisted of final cavity radius and the pressure and integrated impulse at a quartz gauge emplaced in the bottom of the water tank.

The reported calculations were in agreement with this integrated impulse to within 15 percent which is better than the reproducibility of the laboratory record from test to test. However, our calculated cavity radius was approximately 25 percent higher than the average measured value. Even for this larger cavity radius, the calculated cavity pressure before hydrofracture was greater than the average fracture initiation pressure from the laboratory tests (a smaller calculated cavity radius would give a still larger pressure.) From these results and from laboratory experiments showing larger fracture initiation pressures for

faster hydrofractures we concluded that a time-related creep or stress relaxation process must be taking place in the time between the formation of the residual stress field and the hydrofracture of the grout spheres. This relaxation process reduces the magnitude of these stresses so that hydrofracture can occur at lower pressures.

More recent unpublished work at S³ by Bill Proffer and Ed Peterson has identified a plausible mechanism for this relaxation of the residual stress field with time; fluid diffusion from saturated materials under applied stress gradients. A series of calculations made with the GASFLO code (a fluid diffusion code) and the SWIS finite element code have shown that the diffusion of water driven by a residual stress field in grout or tuff can have a dramatic effect in reducing the stress toward the ambient. Within the grout spheres, the relaxation time scale is measured in seconds. In the nuclear case, the calculated time is of the order of months. The results suggest that the residual stress fields being sampled in the grout spheres experiment are the residuum left after the above diffusion process. The nuclear analog would involve a cavity failure many months after the event. We strongly recommend that a way be found to speed up the hydrofrac process by an order of magnitude or so to test this conclusion, one possibility being the use of a gas pressurization system to hydrofracture the exploded spheres.

In recent months, SRI has conducted laboratory tests on configurations other than the standard sphere of 2C4 rock matching grout. Tests have been made in which the PETN sphere was placed inside a larger cavity in the 2C4 grout sphere to simulate a decoupled event. Tests are also being conducted for two different materials, a granite simulant (GS3) and a high void content, low density rock matching grout (LD2C4) formed by adding a specified percentage of hollow silicon microspheres to the usual 2C4 mix. Here, we present the results of our one-dimensional, spherically symmetric, dynamic calculations of the detonation of the PETN explosive and the formation of the compressive residual stress fields around the explosive cavity for these tests.

Calculations were made for the four basic test configurations; (1) the standard 2C4 sphere, (2) the decoupling shot, (3) the low density rock matching grout (LD2C4) and (4) the granite simulat sphere (GS3). All of the calculations gave cavity radii significantly larger than the measured values except for the decoupled shot which gave reasonable agreement. The low-density grout calculation showed the largest cavity radius, the smallest cavity pressure, and the smallest maximum residual hoop stress. The granite simulat calculation gave the smallest cavity, but the largest cavity pressure and residual stress (cavity pressure was greater than 1 Kbar). In all three coupled shots, the maximum residual hoop stress was approximately a factor of two greater than the calculated cavity pressure.

For the decoupled cavity shot the cavity pressure was about a factor of two greater than for the coupled 2C4 test. However, the residual hoop stress for the decoupled cavity test was largest near the cavity and nowhere exceeded the cavity pressure, not an ideal situation for containment. In spite of this, the measured hydrofracture pressures for the uncoupled tests were essentially the same as for the coupled 2C4 experiments. This seems to reinforce the hypothesis that the residual stresses have relaxed with time. However, another possibility exists. Rimer and Friedman⁽⁴⁾ have reported calculations for nuclear events in NTS Area 12 tuff in which the results for coupled and decoupled events are qualitatively similar to the results presented here. These calculations also showed that when the cavity pressure is allowed to decay to zero, the peak residual hoop stress for the coupled and uncoupled cases are very similar and only slightly smaller than for the coupled case before pressure decay.

One disturbing aspect of the calculations is the larger cavity radii (27 percent greater than the measurements for the standard 2C4 sphere). A careful examination was made of the physical dimensions of the experiment including charge weight and density, thickness of lucite shell around the explosive, location of charge relative to the quartz gauge, and material properties of the 2C4 grout. As a result, the

calculational model described in Rimer and Lie⁽³⁾ was altered; the major changes being a reduction in weight of PETN from the nominal 1.375 gms to 1.361 gms, using slightly more lucite, a somewhat different failure envelope for low pressures, and a new location for the quartz gauge at a radius of 6-5/8 inches (16.83 cm) instead of at 7 inches (17.78 cm). The calculated cavity radius decreased only about 2 percent as a result of these changes.

The effect of moving the quartz gauge closer in was to increase the calculated impulse by 42 percent, making it approximately 21 percent greater than the largest reported value and 31 percent greater than the average of the three reported values. Cizek⁽⁵⁾ estimates that the gauge is located at 6-5/8 inches to within a tolerance of $\pm 1/8$ to 1/4-inch. Based on our calculations alone, this implies that the possible error in impulse due to locating the gauge alone may be as great as 15 to 31 percent, irrespective of the reproducibility of the PETN detonation.

SRI has recently performed mechanical properties tests on the three materials of interest, 2C4, LD2C4, and GS3. Tests were conducted of uniaxial compressive strength and splitting tensile strength under both static and dynamic (strain rate of 1.15 or 1.25 sec⁻¹) loading. For all three materials, the tests under dynamic loading conditions showed significantly higher compressive strengths (31 to 61 percent) and tensile strengths (61 to 81 percent).

Our calculations showed strain rates as large as 2×10^5 sec⁻¹ in the sphere of 2C4 grout, several orders of magnitude greater than would be expected in a prototype nuclear or HE event at the same stress levels. The laboratory mechanical properties tests suggest that the grout spheres results cannot be scaled to the large length scales of interest in the nuclear case because of their large strain rates. Our constitutive strength models were changed to take account of the increase in strength of the spheres under higher strain rate loading. This required extrapolating the laboratory strain rate data to the considerably larger strain rates of interest. Calculations made using

this crude dynamic strength model gave cavity radii within 5 percent of the data for all cases except the low-density grout (LD2C4) in which the calculated cavity radius was low by approximately 10 percent.

The larger strengths implied by the dynamic strength model resulted in a significantly narrower positive overpressure pulse at the quartz gauge than obtained with the original strength model and thus smaller peak impulse. The peak pressures were basically the same. Quartz gauge data are available only for the standard 2C4 grout tests and the low density LD2C4 tests. In these cases, the measured durations of positive overpressure were in far better agreement with the calculations using the dynamic strength model than the static strength model. All calculated peak pressures were lower than the data. The calculations using the static strength model gave impulse at the gauges larger than the average data by approximately 10 to 30 percent, but for the dynamic strength model, the impulse was smaller than the data by 30 percent for 2C4 but in good agreement for LD2C4. Since the possible error in impulse due to locating the gauge only to within $\pm 1/8$ to $1/4$ -inch is calculated to be 15 to 30 percent, we feel that too few measurements have been made to evaluate our calculations in terms of impulse.

In summary, the calculations have demonstrated that a higher strength than given by the static laboratory measurements may be needed to match the cavity radius data. Our crude model based on the measured dynamic strengths gives a reasonable match to these data. The higher strength results in larger cavity pressure and higher peak residual stresses. These calculated values are even less consistent with the hydrofracture pressure records even less believable unless some time dependent creep or stress relocation explanation is invoked. This provides further support for our recommendation of a much faster hydrofracture procedure.

The remainder of this report consists of a presentation of the results of our calculations. In Section 2 we discuss our constitutive models for the three grout materials of interest with particular emphasis on the strength modeling. We present detailed results of our calculations in Section 3.

II. CONSTITUTIVE MODELS AND MATERIAL PROPERTIES DATA

In this section, we discuss the constitutive models and material properties used to simulate the behavior of the different grouts used. More complete discussions of the modeling for 2C4 grout and for PETN explosive, lucite and water are contained in Rimer and Lie⁽³⁾. The equation of state for air used for the decoupled calculations is from Alme⁽⁷⁾.

2.1 Laboratory Data

Table 1 gives the physical and mechanical properties data obtained from SRI⁽⁶⁾ for the three materials of interest, the rock-matching grout (2C4), the low-density rock-matching grout (LD2C4) made by combining the basic 2C4 mix with hollow glass microspheres, and the granite simulant (GS3). Additional data available from Terra Tek, Inc. include triaxial compression curves⁽⁶⁾ and uniaxial strain curves⁽¹⁾ for static loading for 2C4 and GS3 only.

The uniaxial compression curves for 2C4 imply 0.7 percent air voids crushed up at approximately 1.4 Kbars as discussed in Rimer and Lie⁽³⁾. Both uniaxial and triaxial data indicate a maximum strength (stress difference) of 0.33 Kb for 2C4 under static loading. We will discuss the dynamic strain rate loading later in this section. For GS3, the uniaxial curves show only 0.5 percent air voids crushed at 0.9 Kb compared with 3.5 percent from Table 1 (calculated from water content and percent saturated data). Triaxial and uniaxial curves at 0.5 Kb confining pressure show stress differences of 1.65 Kb and 1.12 Kb, respectively, but do not indicate a maximum strength value. Little data are available for LD2C4.

These laboratory data were used to construct equations of state for materials 2C4, LD2C4, and GS3. Reasonable assumptions were made where data were lacking.

TABLE 1. PHYSICAL AND MECHANICAL PROPERTIES DATA

Material*	PHYSICAL PROPERTIES										
	Density (g/cm ³)		Water by Wet Weight (%)		Porosity (%)	Saturation (%)	Calculated Air Voids (%)	Longitudinal Velocity (km/sec)	Shear Velocity (km/sec)		
	Wet	Dry	Wet	Grain	(%)	(%)	(%)	(km/sec)	(km/sec)		
2C4	2.16	1.77	18.2	2.88	38	100	0	3.29	1.82		
LD2C4	1.92	1.57	18.4	2.68	42.7	85.1	13.4	3.13	1.78		
GS3	2.42	2.27	6.3	2.80	18.8	81.6	3.5	4.82	2.75		

Material*	MECHANICAL PROPERTIES			
	Unconfined Compressive Strength (psi)* for Given Average Strain Rate (sec ⁻¹)		Splitting Tensile Strength (psi) for Given Average Strain Rate (sec ⁻¹)	
	0.15	0.25	0.15	0.25
2C4	3990	5330	530	900
LD2C4	3200	5000	500	800
GS3	9210	14000	920	1620

* 2C4 = Rock-Matching Grout
 LD2C4 = Low-Density Rock-Matching Grout
 GS3 = Granite Simulant
 1 psi = 6854.76 Pa
 1 bar = 10⁵ Pa

More recently, Cizek and Florence⁽⁸⁾ have reported strength measurements which are the average of a set of laboratory measurements for each of the three materials. In some cases, these measurements differ from the earlier numbers shown in Table 1. They are reported in Table 2 for completeness but did not influence the construction of our equations of state. Following is a summary of the equations of state used for the three materials of interest.

2.2 Rock-Matching Grout Model (2C4)

Table 3, reproduced from Rimer and Lie⁽³⁾ summarizes the material properties data used for the early 2C4 grout calculations while Figure 1 gives the load-unload curves (porous crushup) for this material. The strength parameters shown in Table 3 are from a parabolic variation of yield strength with P, defined by

$$\bar{P} = P - \frac{1}{2} \left(\frac{J_3'}{2} \right)^{1/3},$$

where P is the mean stress and J_3' the third deviatoric stress invariant. These parameters give a maximum stress difference ($Y_o + Y_m$) of 0.33 Kb reached at \bar{P} equal to 0.4 Kb and also correspond to an unconfined compressive strength of 0.279 Kb (approximately 4000 psi). Both maximum strength (stress difference) and unconfined strength are in agreement with the laboratory data for 2C4. However, the maximum possible tensile strength of 0.263 Kb (in a hydrostatic state of stress) is much greater than given by the laboratory data (approximately 0.036 Kb). The model (no tensile failure without shear failure first) for other stress states does permit tensile failure in a principal direction at lower tensile stress values (for example, approximately 105 bars for a state of pure shear).

A straight line variation between yield strength and \bar{P} up to a maximum strength of 0.33 Kb was used for the present study. This new failure surface given by

$$Y = 0.055 + 1.6 \bar{P} \text{ (kb)}$$

TABLE 2. AVERAGE STRENGTHS OF RMG 2C4, LD2C4, and GS3 (Reproduced from Cizek and Florence⁽⁸⁾)

<u>Material</u>	<u>Average Strain Rate (sec⁻¹)</u>	<u>Compressive Strength (psi)</u>	<u>Tensile Strength (psi)</u>
RMG 2C4	Static	3990	580
RMG 2C4	0.15	5330	900
LD 2C4	Static	3200	520
LD 2C4	0.15	5000	780
GS3	Static	9210	920
GS3	0.15	15,900	1620

Table 3. Summary of 2C4 Grout Material Properties Data.

<u>Quantity</u>	<u>Symbol</u>	<u>Value</u>	<u>Units</u>
Longitudinal sound speed	C	3.27	km/sec
Shear wave speed	C _s	1.82	km/sec
Density	ρ ₀	2.16	gms/cc
Zero pressure bulk modulus	K ₀	135.57	kbars
Shear modulus	G	71.55	kbars
Poisson's ratio	σ	0.275	
Coefficients for Tillotson Equation of State	A	150	kbars
	B	335	kbars
	β ₁	5	
	β ₂	5	
	a	0.5	
	b	0.633	
	e ₀	6.0x10 ¹¹	ergs/gm
Strength Parameters	e _{s1}	3.5x10 ¹⁰	ergs/gm
	e _{s1}	1.8x10 ¹¹	ergs/gm
	Y ₀	0.21	kbars
	Y _m	0.12	kbars
Air-filled Porosity	ν _m	0.40	kbars
	e _m	2x10 ¹⁰	ergs/gm
	e _m		
Elastic Pressure	φ ₀	0.007	
Crush Pressure	p _e	0.1	kbars
	p _c	1.4	kbars

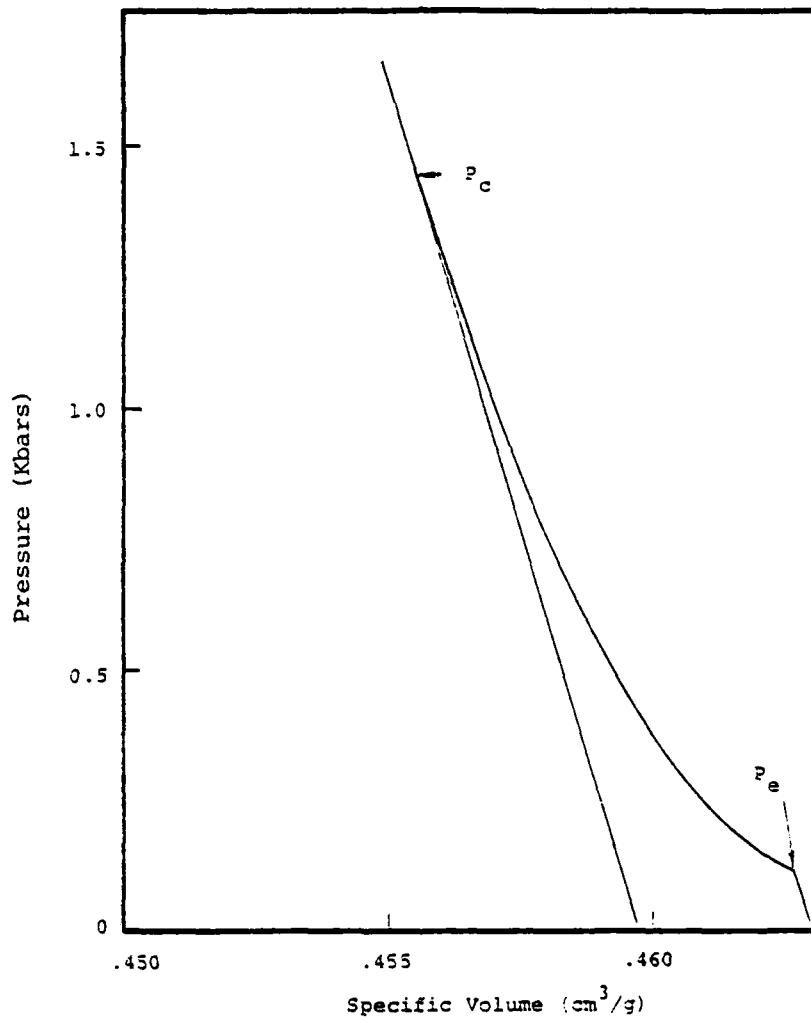


Figure 1. Load-unload curves for 2C4 grout.

is consistent with both the laboratory values of unconfined compressive strength and tensile strength for 2C4 grout. Figure 2 shows a comparison between the old and new failure surfaces.

2.3 Granite Simulant Model (GS3)

Whenever possible, laboratory data were used in developing the constitutive model for the granite simulant. Thus, the density and elastic parameters for GS3 come directly from Table 1 as does the calculated air voids of 3.5 percent. The uniaxial strain load-unload curve⁽¹⁾ showed only 0.5 percent air voids crushed up at a mean stress of 0.9 Kb. Assuming that the calculated air voids indicated a considerably higher crush pressure, we used the 0.5 percent air void at 0.9 Kb as one point on the loading curve shown in Figure 3. The loading curve above the crush pressure was a straight line with bulk modulus of 335 Kb.

In a recent conversation, J. C. Cizek of SRI has brought into question the saturation data for GS3 given in Table 1. The experimental procedure is to maintain the GS3 sphere in a water bath at all times. Therefore, Cizek believes that the granite simulant is fully saturated, and that the air-filled voids are negligible. This information came too late to be included in our constitutive model and calculations. However, we believe that since GS3 was not mixed in a vacuum, air bubbles were entrained which could result in a few percent air-voids. The water bath could not remove such bubbles.

If the simulant were truly 100 percent saturated, we would anticipate a slightly larger cavity radius than calculated with our model. However, the measured cavity radius was actually smaller than calculated. The absence of air-filled voids would increase the pressure and impulse at the quartz gauge greatly. No data are available for comparison.

The measured unconfined compressive strength, tensile strength and stress difference at 0.5 Kb confining pressure under triaxial loading were used to determine the coefficients of a parabolic failure surface

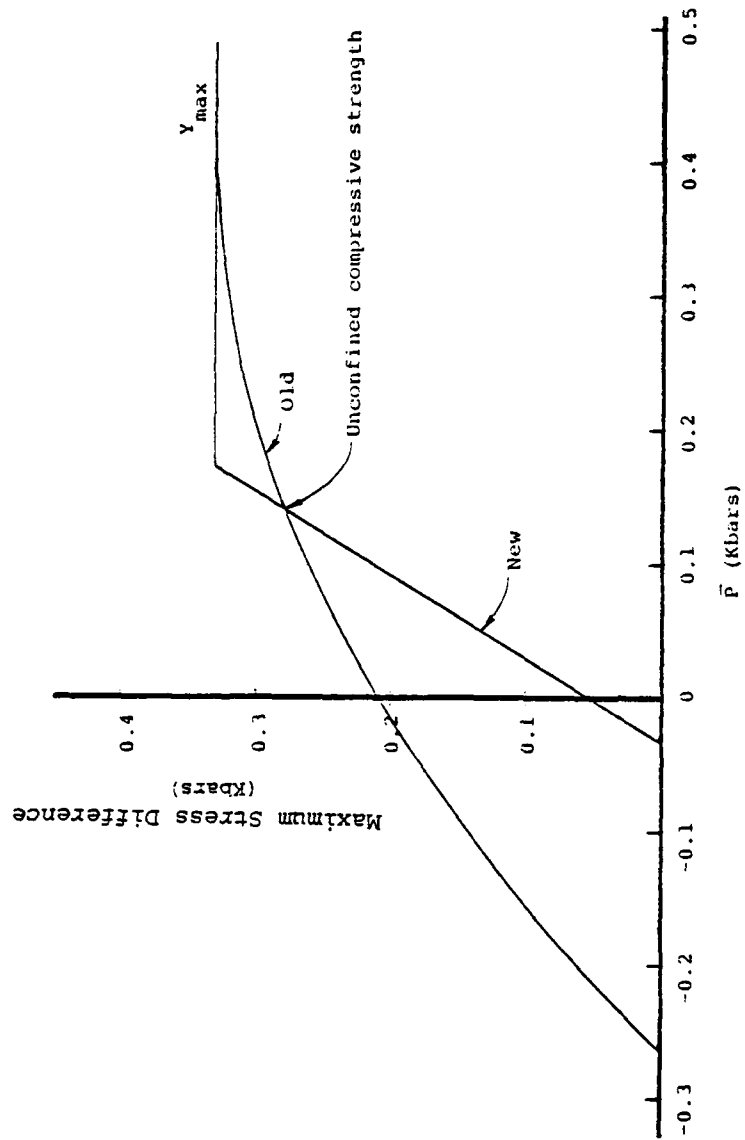


Figure 2. Old and new failure surfaces for 2C4 grout.

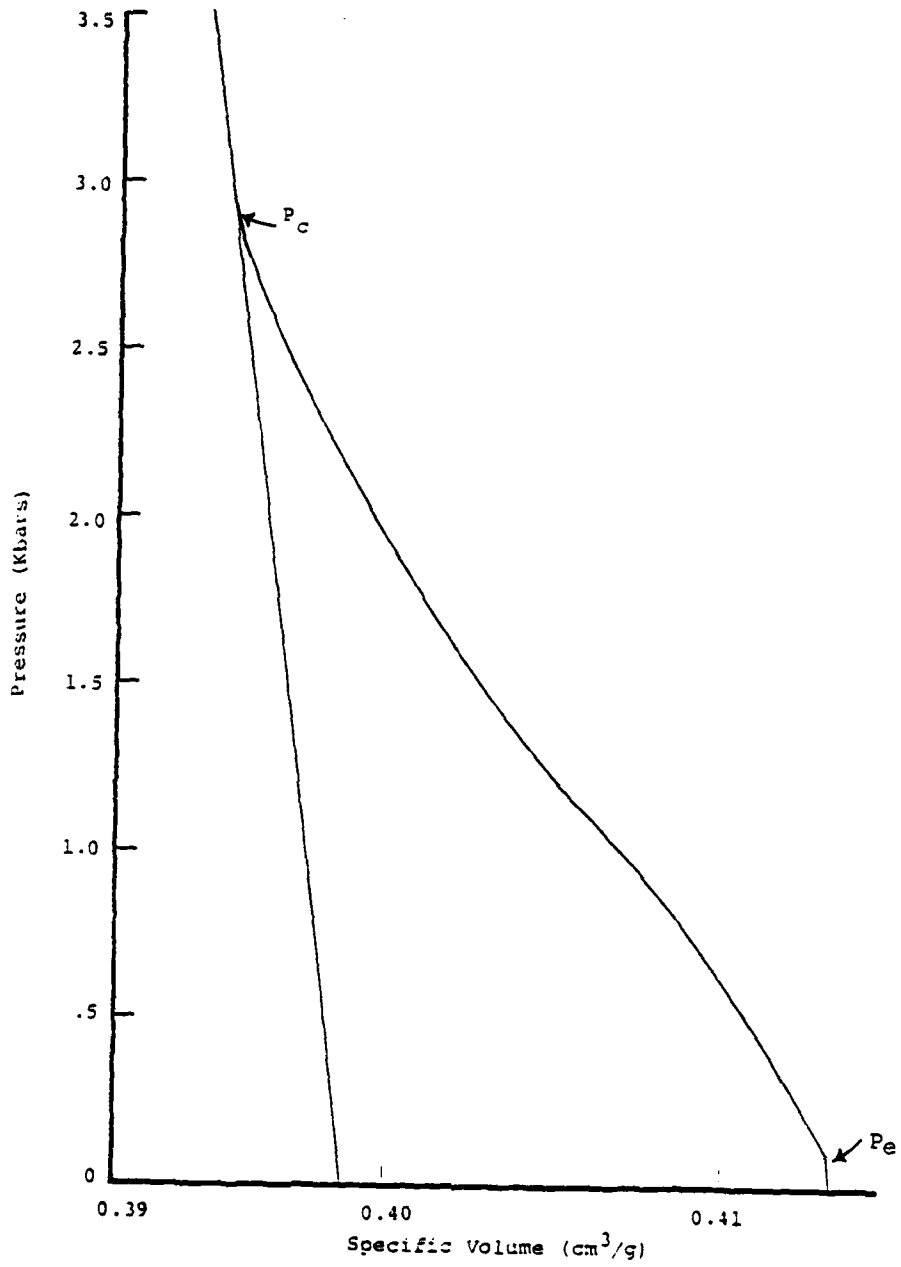


Figure 3. Specific volume load-unload curves for granite simulant (GS3).

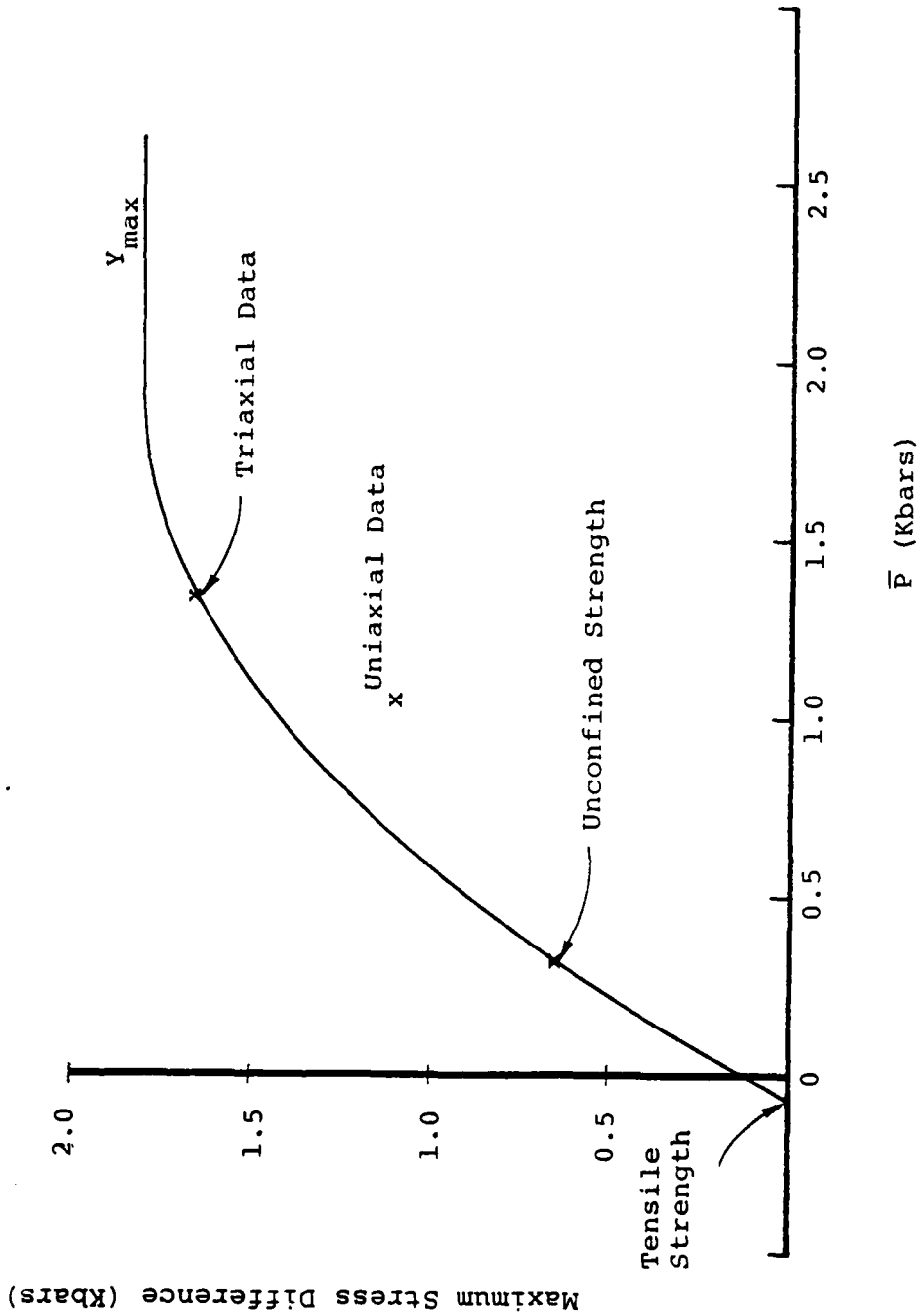


Figure 4. Failure surface for granite simulant GS3

(vs \bar{P}) for static loading conditions. Since the uniaxial loading data did not show a clear maximum stress difference, and since no other data were available, we extrapolated the parabolic form of the failure surface to obtain a maximum stress difference of 1.795 Kb, only 9 percent greater than the given triaxial measurement. Figure 4 shows our failure surface for GS3. Note that the uniaxial data (at 0.5 Kb confining pressure) is below the failure surface.

2.4 Low Density Rock Matching Grout Model (LD2C4)

The low density rock matching grout (LD2C4) was made by blending the standard 2C4 mix with a specified amount of Q-CEL microspheres which encapsulate air in hollow spherical shells derived from inorganic silicate. Our first model utilized the sparse preliminary data available at that time (13.4 percent air voids and a density of 1.92 gms/cm³) and filled in the gaps by using the material properties developed for 2C4. Thus, the crush pressure P_c , the elastic pressure P_e and the general shape of the load-unload curves shown in Figure 5 are similar to Figure 1. The straight line failure surface of Figure 2 was used for the first LD2C4 grout spheres calculation.

Our present model incorporates the later data shown in Table 1. The major changes from the preliminary model are in the failure surface, given by

$$Y = 0.0525 + 1.52 \bar{P} \text{ (Kb)}$$

with a specified maximum strength of 0.26 Kb, which is approximately 20 percent smaller than before, and in the load-unload curve. We felt that the crush pressure should be considerably larger because of the large amount of air-filled voids. Retaining the same general shape for the load curve gave us the present curve shown in Figure 5.

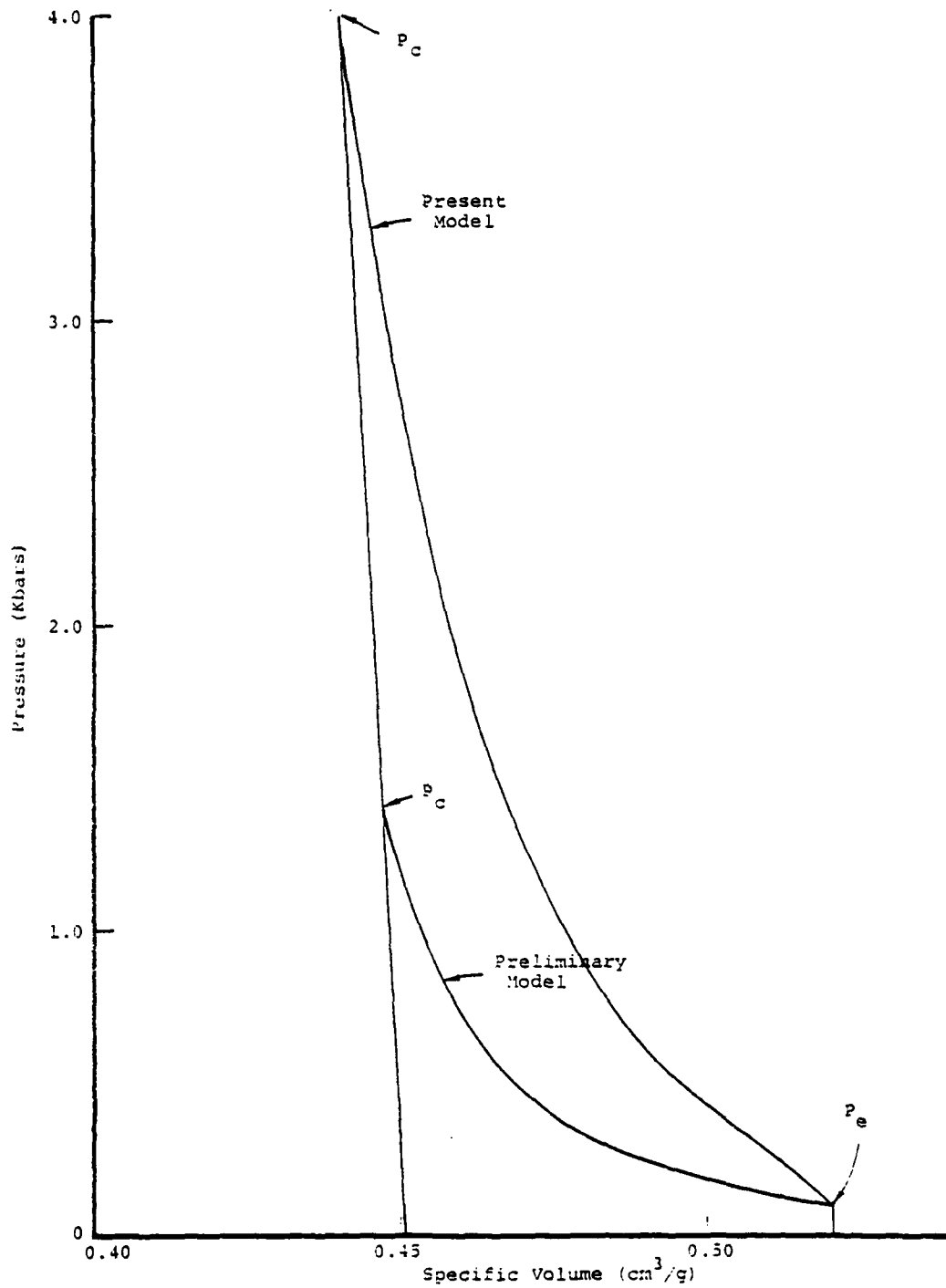


Figure 5. Load-unload curves for low-density rock-matching grout LD2C4.

2.5 Dynamic Strength Models

Table 1 gives the values of unconfined compressive strength and tensile strength for the three materials of interest for both static and dynamic loading. (The average strength values shown in Table 2 came too late to be included in our models.) For our purposes, we assumed that the "static" loading was represented by an average strain rate of 0.001 sec^{-1} . Thus, the "dynamic" loadings correspond to approximately two orders of magnitude greater strain rates. At these higher strain rates, the unconfined compressive strength was increased by 30 to 60 percent (depending on the particular material) while the tensile strength was increased by 60 to 80 percent. Since no laboratory data were available on increased shear strength at confining pressure, we decided to assume that maximum strength (stress difference) was increased by the same percentage as the unconfined strength.

The classical theory for metals assumes that strength increases linearly with the logarithm of strain rate. Our grout spheres calculations have shown strain rates of the order of 10^5 sec^{-1} , eight orders of magnitude greater than the assumed static loading data and approximately 6 orders of magnitude greater than the dynamic loading data of Table 1. Thus the strain rate model must extrapolate the existing data over many orders of magnitude and, therefore, could be quite inaccurate. The difference between using the data of Table 1 or Table 2 when extrapolated to higher strain rates, could be significant. However, we hoped that our model would show us whether or not strain rate effects could bring the calculated cavity radii into better agreement with the measurements.

Our model assumes that at all strain rates the functional form of the failure surface (straight line for 2C4 and LD2C4 and parabolic for GS3) does not vary. For a given time and Lagrangian position, the failure surface (stress difference as a function of P) is defined by the radial strain rate in the computational cell. Deviatoric stresses at

this time and position are limited to the present failure surface as described in Rimer and Lie³. At the next instant of time, the failure surface for the cell will change if the strain rate varies.

The constants defining the functional form are themselves defined as functions of strain rate. For example, we have already defined a simple failure surface for 2C4 grout under static loading (0.001 sec^{-1}) using three constants, a stress difference at zero P, a slope of the straight line segment, and a maximum stress difference. We use the data from Table 1 for a strain rate of 0.15 sec^{-1} to define a similar failure surface for that strain rate and relate the three constants (functions of strain rate) by assuming linear variations of these constants with logarithm of the strain rate. For the granite simulant GS3, the procedure is similar except that a parabolic form is assumed. Table 4 defines the strain rate dependence for the three materials of interest.

III. CALCULATIONAL RESULTS

3.1 Description of Calculations

Table 5 describes and summarizes the results of the calculations made using the spherically symmetric SKIPPER code. In this table, static failure refers to the standard failure model based on data from laboratory tests under static loading conditions while dynamic failure refers to the model presented in section 2.5 which used the laboratory data under dynamic loading conditions presented in Table 1. Calculations 1 through 4 were made using the model for the explosive lucite sphere described in Rimer and Lie³, i.e., exactly 0.375 gm of PETN, outer radius of 0.447 cm, surrounded by lucite out to a radius of 0.476 cm. All calculations were for a grout sphere 15.24 cm in radius, surrounded by water at a pressure of 1000 psi (approximately 69 bars). For the first four calculations, the quartz gauge was modeled as being 7 inches from the center of the sphere. For all other calculations, the gauge was at 6-5/8 inches.

TABLE 4. DEPENDENCE OF FAILURE SURFACES ON STRAIN RATE

2C4

$$Y = 0.055 f_1 + 1.60 f_2 \bar{P} \text{ (Kb)}$$

$$Y_{\max} = 0.33 f_3 \text{ (kb)}$$

$$f_1 = 1 + 0.32 \bar{\epsilon}$$

$$f_2 = 1 - 0.0287 \bar{\epsilon}$$

$$f_3 = 1 + 0.155 \bar{\epsilon}$$

where

$$\bar{\epsilon} = \log_{10} (\text{strain rate}/0.001)$$

LD2C4

$$Y = 0.0525 f_4 + 1.52 \bar{P} \text{ (Kb)}$$

$$Y_{\max} = 0.26 f_5 \text{ (Kb)}$$

$$f_4 = 1 + 0.245 \bar{\epsilon}$$

$$f_5 = 1 + 0.237 \bar{\epsilon}$$

GS3

$$Y = 0.115 f_6 + \frac{1.68 f_8}{1.88 f_7} \bar{P} \left[2 - \frac{\bar{P}}{1.88 f_7} \right] \text{ (Kb)} \quad \bar{P} < 1.88 \text{ (Kb)}$$

$$Y_{\max} = 0.115 f_6 + 1.68 f_8 \text{ (Kb)} \quad \bar{P} \geq 1.88 \text{ (Kb)}$$

$$f_6 = 1 + 0.317 \bar{\epsilon}$$

$$f_7 = 1 + 0.483 \bar{\epsilon}$$

$$f_8 = 1 + 0.439 \bar{\epsilon}$$

TABLE 5. SUMMARY OF RESULTS OF CALCULATIONS

Run Description	Cavity Radius (cm)		Cavity Pressure (bars)	Peak Residual Stress (σ_r bars)	Gauge Location (inches)	Peak Reflected Pressure (bars) Calc.	Peak Reflected Impulse (bars- μ sec) Calc.	Peak Reflected Data
	Calc.	Data						
STATIC FAILURE								
1. 2C4	1.21	0.95 (Avg)	256	447	7	46.5 (70 Avg)	766	760-900 (690)
2. Decoupled 2C4	1.12	1.07, 1.21, 1.23	604	605	7	23.5	320	825 (Avg)
3. GS3	0.81	0.64	1160	1345	7	22.5	210	-
4. Preliminary LD2C4	1.29	1.14-1.21	196	270	7	5.5 (17.2)	155	200-350 (190)
5. 2C4 (less PETN)	1.19	0.95	259	424	6-5/8	50.5	090	760-900 (690)
6. LD2C4	1.30	1.14-1.21	186	300	6-5/8	12.5 (17.2)	380	200-350 (190)
DYNAMIC FAILURE								
7. 2C4	0.99	0.95	512	743	6-5/8	46.5	500	760-900 (690)
8. Decoupled 2C4	1.04	1.07, 1.21, 1.23	743	643	6-5/8	24.5	218	-
9. GS3	0.665	0.64	2840	2840	6/5/8	22.4	142	-
10. LD2C4	1.04	1.14-1.21	434	617	6-5/8	17.3 (17.2)	246	200-350 (190)

() indicates latest quartz gauge data as of November 25, 1979. (SRI Himenthly)

As described in Section 2.2., the material properties used in Calculation 1 differed from those of Reference 3 only in the shape of the failure surface for 2C4 grout. The results of this calculation were essentially the same as reported earlier (peak reflected impulse increased from 735 to 766 bars- μ sec). Calculation 2 used the same material properties but modeled air between the lucite shell and the 2C4 grout at a radius of 0.95 cm. For this decoupled test, we initialized the stress distribution in the grout using the Lamé solution for a hollow elastic sphere pressurized from the outside. Calculation 3 used the material properties for the granite simulant GS3 discussed in Section 2.3 while Calculation 4 incorporated the preliminary model for LD2C4 grout from Section 2.4.

For Calculation 5, the mass of PETN explosive was reduced slightly to 0.360 gm and the lucite sphere was given an outer radius of 0.482 cm reflecting more current information about the SRI tests. These changes only insignificantly altered the calculational results in the grout when compared with Calculation 1. However, another change, moving the simulated location of the quartz gauge in to 6-5/8 inches (16.8 cm), gave a large increase (42 percent) in the calculated reflected impulse. (This result will be discussed in some detail later in this report.) All subsequent calculations used this gauge location and the charge configuration of Calculation 5. Calculation 6 used more recent laboratory data to better define the constitutive model for LD2C4 grout. These resulted in a lower shear strength and less easily crushable air-filled voids.

Calculations 2, 3, 5 and 6 include our best estimates at present of the constitutive models and material properties for the tests of interest based on the standard laboratory materials tests. Because of the lack of agreement with some of the SRI test results the constitutive model described in Section 2.5 was developed to simulate the effect of dynamic (i.e., strain rate dependent), loading on the shear failure of the grouts tested. Calculations 7 through 10 of Table 5 were made using this "dynamic failure" model.

3.2 Comparisons Between Calculations and Cavity Radius and Quartz Gauge Data

Unfortunately very little experimental data exist which is directly comparable to the calculations. We can compare calculated and measured cavity radii for all four of the experimental configurations of interest, coupled and decoupled 2C4 grout, granite simulant GS3 and low density grout, LD2C4. However, quartz gauge data are only available at the present time for the 2C4 and LD2C4 grout configurations.

Table 5 summarizes many of the calculational results and compares them with the measurements. In general, for the static failure model, (Calculations 1 through 6) calculated cavity radii are considerably greater than the measured values, the only exception being the decoupled 2C4 cavity where the calculated radius is within the range of the data. Using our strain rate dependent failure surface to increase the shear strength (Calculations 7 through 10) in all cases resulted in a lower calculated cavity radii than for the failure surfaces based on static laboratory tests. The three coupled calculational configurations gave decreases of approximately 20 percent in cavity radius while the decoupled 2C4 cavity (where shear failure is relatively insignificant) decreased in radius less than 8 percent. For both the coupled 2C4 and the GS3 configurations, the resulting cavity radii were within 5 percent of the experimental measurements. However, the LD2C4 grout calculations which showed the largest decrease in cavity radii due to dynamic effects, gave significantly smaller radius than the data. This may be due to the extrapolation of strength data based on Table 1 rather than the later data of Table 2. Taken as a whole, the results using our crude dynamic failure model, which extrapolates the laboratory data many orders of magnitude in strain rate, indicate the importance of strain rate dependent effects in these small scale laboratory experiments. Our guess is that these effects would be insignificant for the prototype nuclear tests in which strain rates may be three orders of magnitude lower.

Figure 6 shows the pressure-time record at the quartz gauge in the floor of the water tank for 2C4 grout Test 157 together with the simulated records for Calculations 1, 5, and 7. Test 157, the most recent

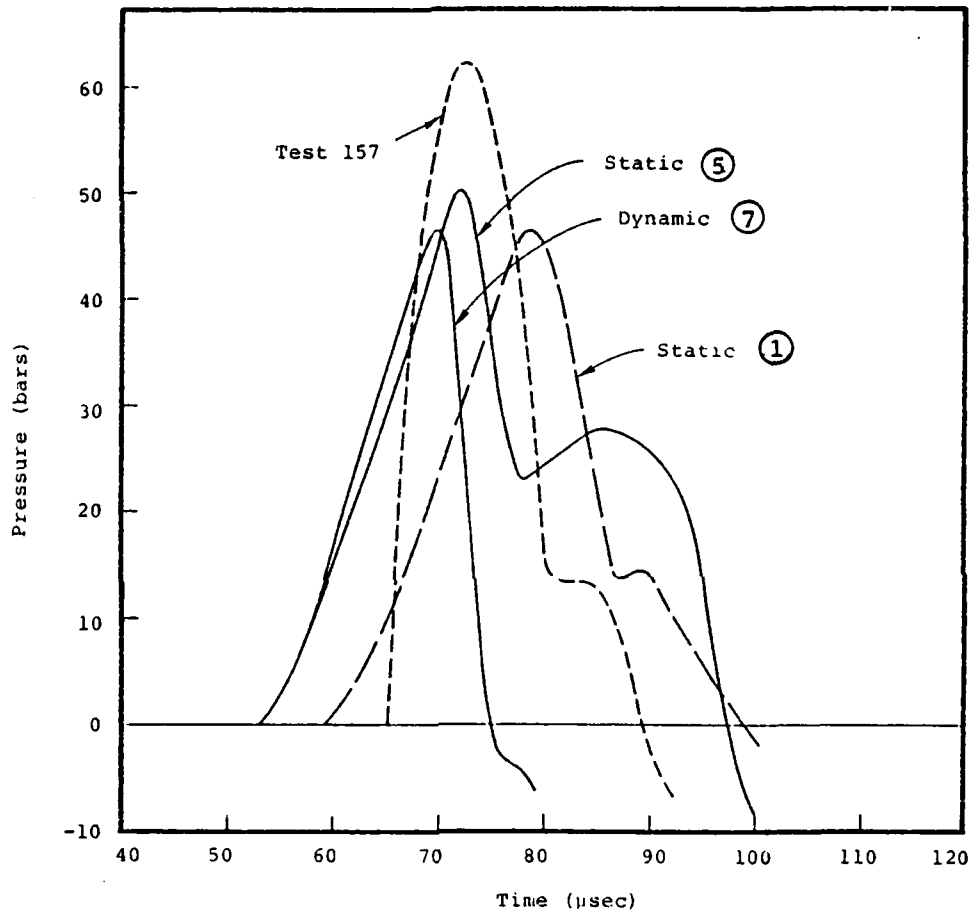


Figure 6. Comparison between quartz gauge record (Test 157, Impulse = 761 bars-μsec) and calculations for 2C4 grout.

of the three available quartz gauge records, gave the smallest integrated impulse of 751 bars- μ sec (the maximum was 896 bars- μ sec). The gauge is nominally located 6-5/8 inches from the center of the explosive but only to within \pm 1/8 to 1/4 inch. Calculation 1 placed this gauge at 7 inches while Calculations 5 and 7 located it at 6-5/8 inches. All three calculations show an earlier signal arrival due to numerical diffusion. A more valid comparison is between the times of arrivals of the peak (reflected) pressures. Calculation 1 has the peak arriving too late; Calculation 5 has the same arrival as the data; and Calculation 7 (the dynamic failure model) has a slightly early arrival. All calculations for 2C4 grout show a lower peak pressure than the gauge record. However, the shapes of the calculated pulses and the impulse derived from them vary greatly. Calculation 1 has the same shape as the characteristic gauge record, i.e., a rise to the peak followed by a fall to a plateau and a further fall-off. Calculation 5, for the closer-in gauge location and the slightly different charge configuration, shows a rise to a second peak following the fall-off which appears to be due to a small second pulse (present in Calculation 1 as well) which is in phase with the reflected main pulse at the gauge for this particular gauge location. This small pulse appears to be a reflection from the lucite PETN interface which has rebounded at the origin and is propagating radially outward. Neither a plateau nor second peak is visible in the pulse from Calculation 7 for the dynamic failure model. The pressure record from Calculation 7 would give an impulse in excellent agreement with the data if a plateau such as in Calculation 1 was present. Table 5 shows comparisons between the simulated and experimentally derived impulses. Calculation 1 gives excellent agreement (it has a wider pulse but lower peak) with the data, while Calculation 5 gives significantly larger impulse due to the second peak.

Figure 7 compares the quartz gauge records from tests 201 and 202 with three calculations for LD2C4 grout, the preliminary model (Calculation 4) with gauge location at 7 inches, the later model with static

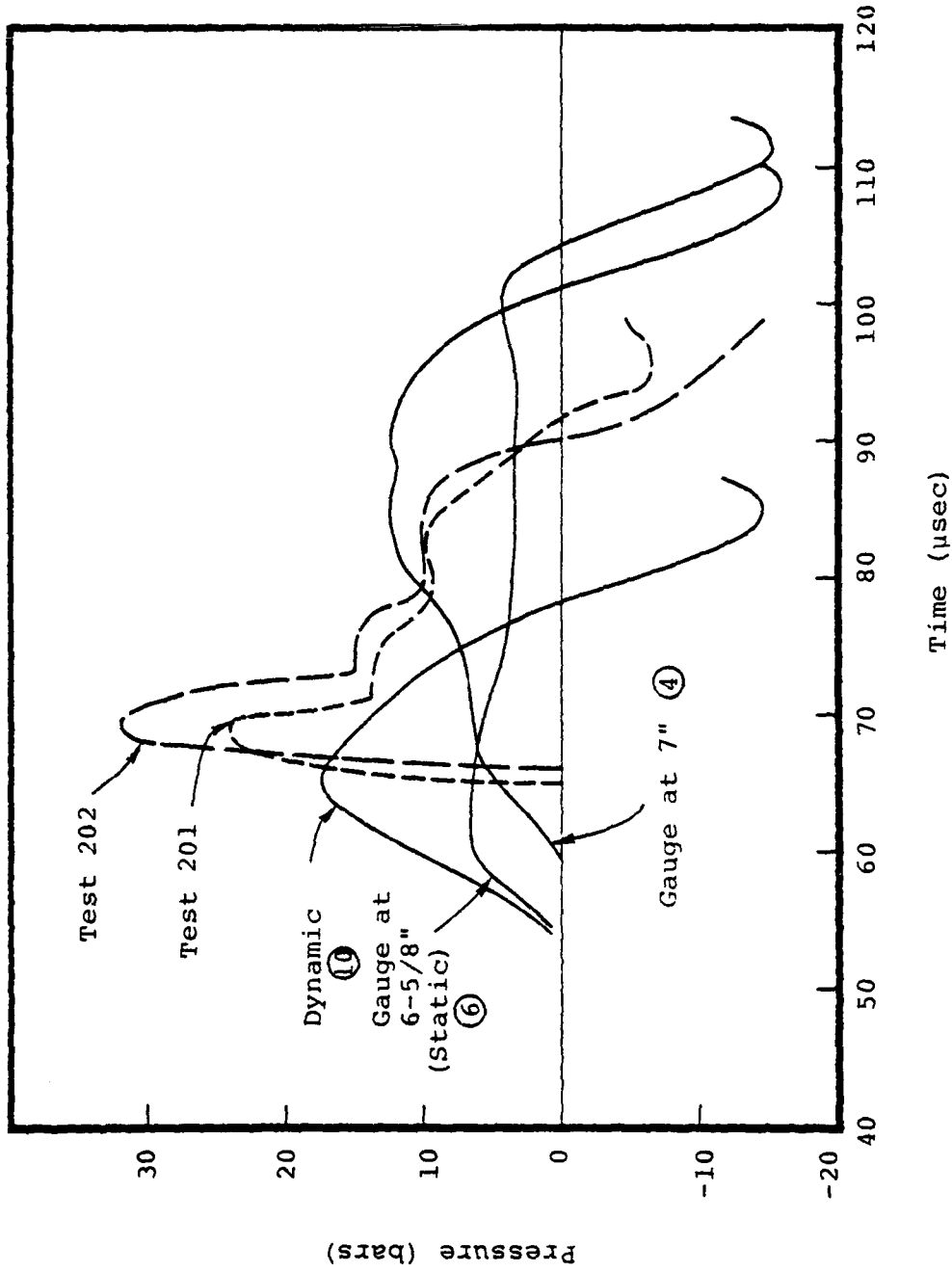


Figure 7. Comparison between quartz gauge records (Tests 201 and 202) and calculations for LD2C4 group.

failure data (Calculation 6) and with dynamic failure data (Calculation 10) both with the gauge location at 6-5/8 inches. As was true for 2C4 grout comparisons, arrivals are earlier than the data. Both Calculations 4 and 6 (the static failure model) show much larger pulse widths than the gauge records. However, the dynamic failure model gave a pulse width in excellent agreement with the data. Again, the dynamic model gave a pulse shaped differently than the data. Tests 201 and 202 (the early records sent to us) used spheres of LD2C4 grout that had higher than normal densities. Cizek⁽⁹⁾ describes the standard LD2C4 mix (density 1.9) as giving considerably lower peak pressures (17 bars) and maximum impulses (200 bars- μ sec) than these tests and having a shape similar to the 2C4 records. The pulse of Calculation 10 (the strain-rate dependent model) is in excellent quantitative agreement with the results from the tests using the standard LD2C4 mix.

Figure 8 shows the calculated pressure vs time for the granite simulant GS3 for the static model (gauge at 7 inches) and the dynamic failure model (gauge at 6-5/8 inches). Figure 9 shows similar curves for the decoupled 2C4 calculations. In both figures, the only noticeable differences between static and dynamic failure models are the earlier arrivals due to change in gauge location and the narrower pulses for the dynamic models. No data are available for comparison.

3.3 Discussion of Results

The major purpose of the grout spheres tests was to evaluate the importance of the explosively produced compressive residual stress fields on containment of the cavity gases. We believe that due to a time dependent stress relaxation mechanism the residual stresses of interest are no longer present in the laboratory experiments at the time of hydrofracture. However, we hope that our calculations, together with the existing laboratory data, may prove useful in comparing containment prospects for the four laboratory configurations, in order to extrapolate the results to nuclear test media.

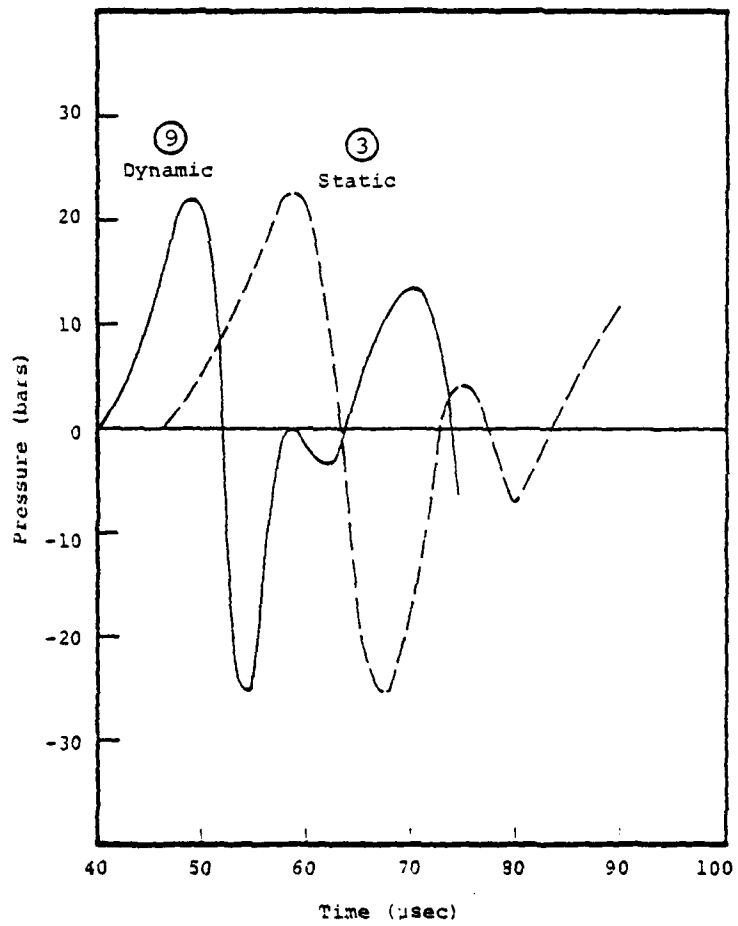


Figure 8. Simulated quartz gauge records for granite simulant GS3 tests.

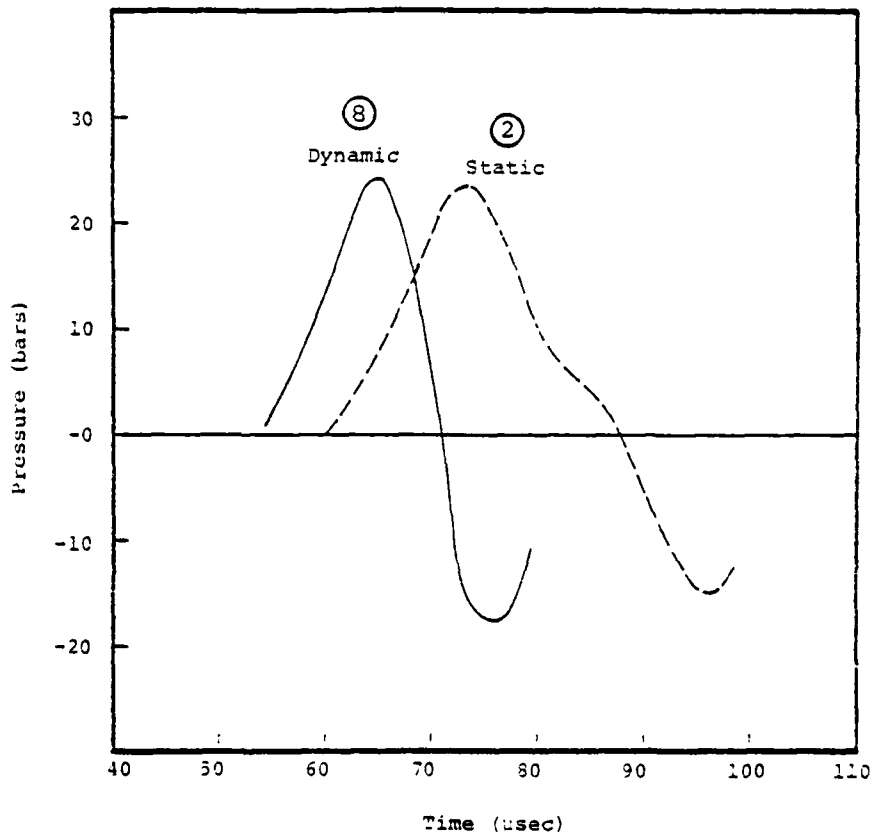


Figure 9. Simulated quartz gauge records for decoupled 2C4 grout tests.

Figure 10 gives the calculated peak stresses (relative to the 69 bar overburden) vs range from all of the calculations for the static model (Calculations 1 and 5 overlay) and from Calculation 10 for LD2C4. The plots for static and dynamic loading for all configurations were very similar down to 0.5 Kb or less when strength effects become significant. Since the magnitude of residual stress fields has been shown (see Rimer⁽¹⁰⁾) to be very dependent on yield strength, peak stress alone is not a good indication of containment. The situation is further complicated by the effects of other material properties on cavity size, cavity pressure, and stress levels.

Let us compare the results of Table 5 and Figure 10 first for LD2C4 grout. Calculation 4 (the preliminary model) and Calculation 6 (the later model) show very similar peak stresses down to approximately 10 Kbar (the higher stress levels are dominated by air-filled voids which are the same for both). However, in the range between 1 and 10 Kb, the results differ because of the different crush pressures used. Calculation 6 shows a noticeable increase then decrease in slope in the peak stress curve at a stress level of 5 Kb (the crush pressure is 4 Kb) while Calculation 4, for a crush pressure of 1.4 Kb (also a 20 percent lower strength), shows this phenomena at a lower stress level. The result is considerably more air-voids crushed up for Calculation 4 and lower peak stress, impulse, etc. Even though more voids are crushed, the cavity is slightly smaller (and cavity pressure is higher) due to the higher strength used in Calculation 4 so that the ratio of peak residual hoop stress to cavity pressure, assumed here to be a rough containment guide, is lower. Calculation 10, identical to Calculation 6 except for the stronger failure surface, shows a factor of 2 higher residual stresses but also a greater than factor of 2 increase in cavity pressure. In fact, the trend for all tamped configurations is that the dynamic model results in lower ratios of peak residual hoop stress to cavity pressures.

Primarily due to the lower air-void content, the 2C4 calculations show considerably larger peak stresses at all ranges and smaller cavities than for LD2C4. Approximately the same ratios of peak residual

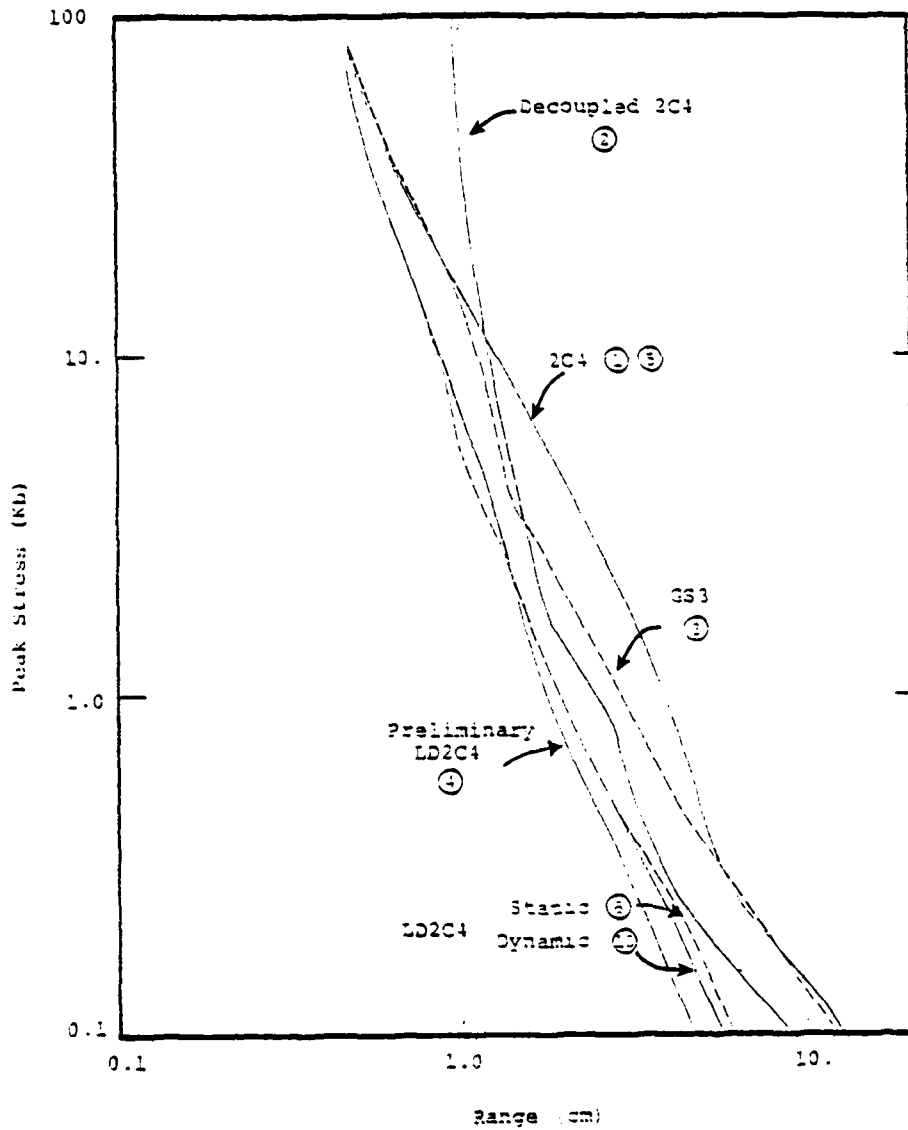


Figure 10. Peak stress (overstress) vs range for 2C4, decoupled 2C4, LD2C4 (preliminary, final static and dynamic models) and GS3 spheres using static failure data.

hoop stress to cavity pressure are seen. The granite simulant GS3 sphere has a volume of air-filled voids intermediate between 2C4 and LD2C4 so that the peak stress vs range curve lies in between the other two configurations over the stress regime where the effects of voids dominate. Once again, changes in slope are seen at peak stresses around the crush pressure of 3 Kb, but at stress levels below 0.3 Kb the curve is almost identical to the 2C4 curve. The high strength of GS3 results in very small cavities, very large cavity pressures, and very high residual stresses when compared with the other configurations. However, the ratio of peak residual hoop stress to cavity pressure is smaller, which may indicate worse containment prospects.

Calculations 2 and 8, for the decoupled configuration, give somewhat different results. In Figure 10, peak stresses are much higher in close due to the impact of the shocked air on the walls of the decoupled cavity and attenuation is much steeper. The cavity expands only slightly from its initial radius of 0.95 cm. As a result, considerably less plastic yielding occurs around it.

Figures 11 and 12 show the residual stress fields calculated for the decoupled 2C4 spheres using the static and dynamic failure models, respectively. Figures 13 and 14 show similar plots calculated for the coupled 2C4 spheres while Figures 15, 16, 17 and 18 show plots for the coupled LD2C4 and GS3 spheres. The times at which the stress fields are monitored are included since elastic rebounds due to the simulated tank wall are present which modify these fields out to much later times. (These rebounds may change the peak residual stresses from the values shown by ± 10 percent.) In all cases studied, the peak residual stresses are both greater for the dynamic failure model than for the static model and are located at smaller radial distances. The coupled grout spheres show peak residual hoop stress significantly greater than the peak radial stress. However, the decoupled calculations, due to the smaller cavity expansion and less plastic yielding, give residual stresses that appear to be more like the elastic solution, i.e., both maximum hoop stress and radial stress located at or near cavity boundary and radial stress greater than hoop stress over the ranges of interest.

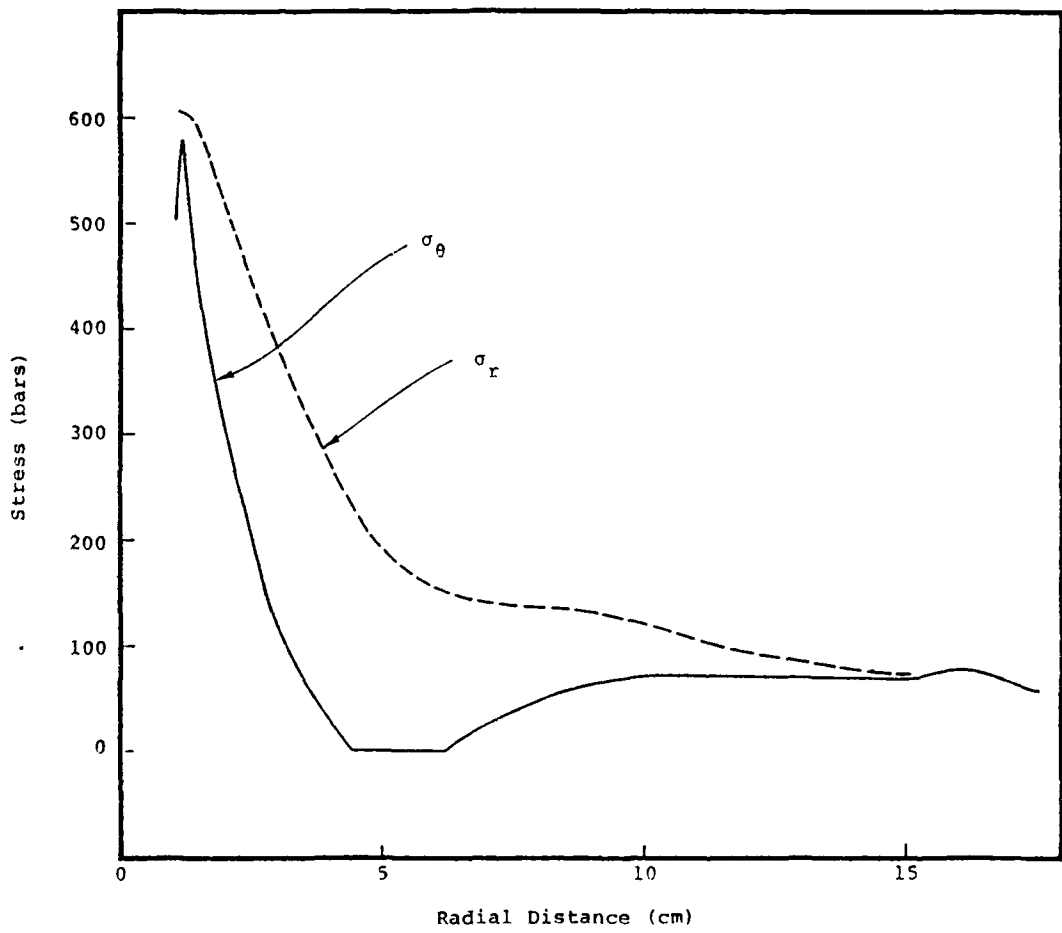


Figure 11. Residual stress fields at 99 μ sec for decoupled 2C4 calculation 2 (static failure model)

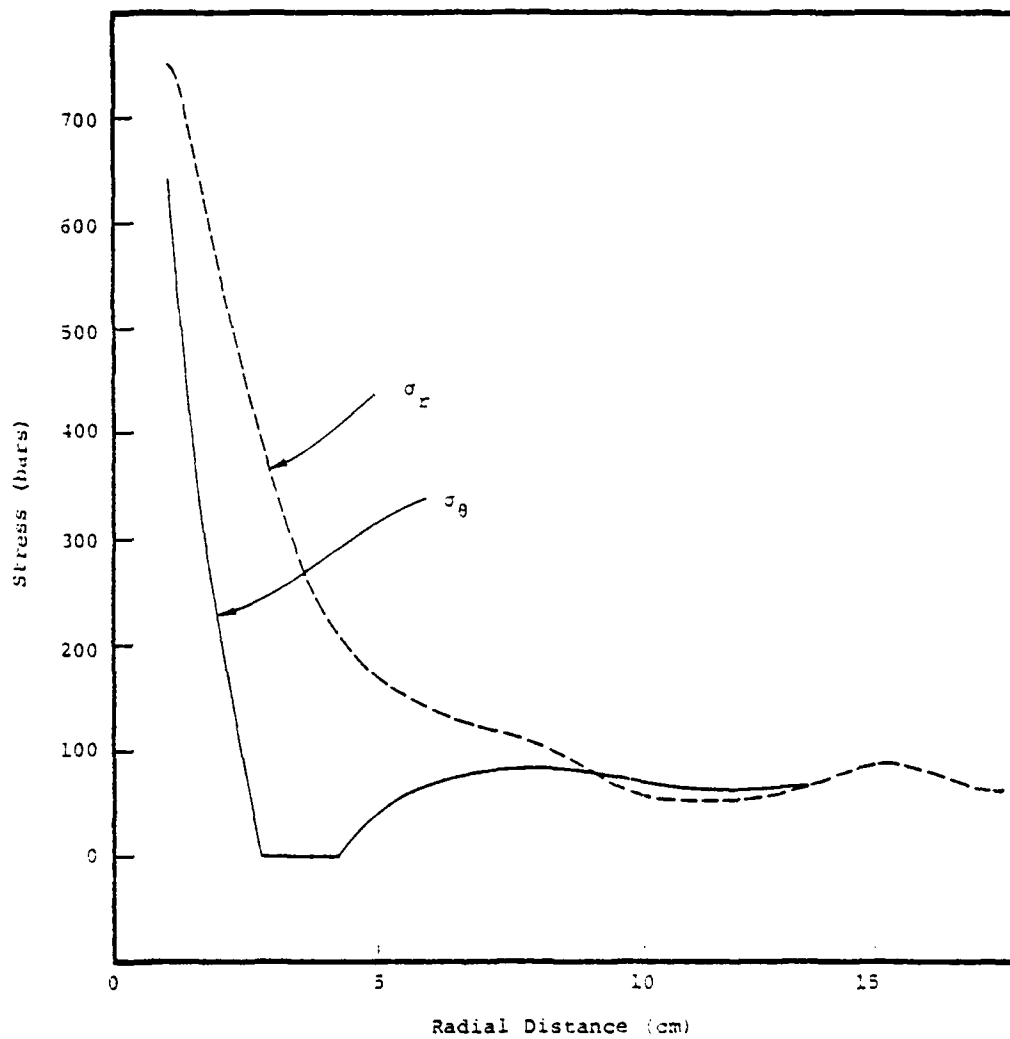


Figure 12. Residual stress fields at 100 μ sec for decoupled 2C4 calculation 8 (dynamic failure model).

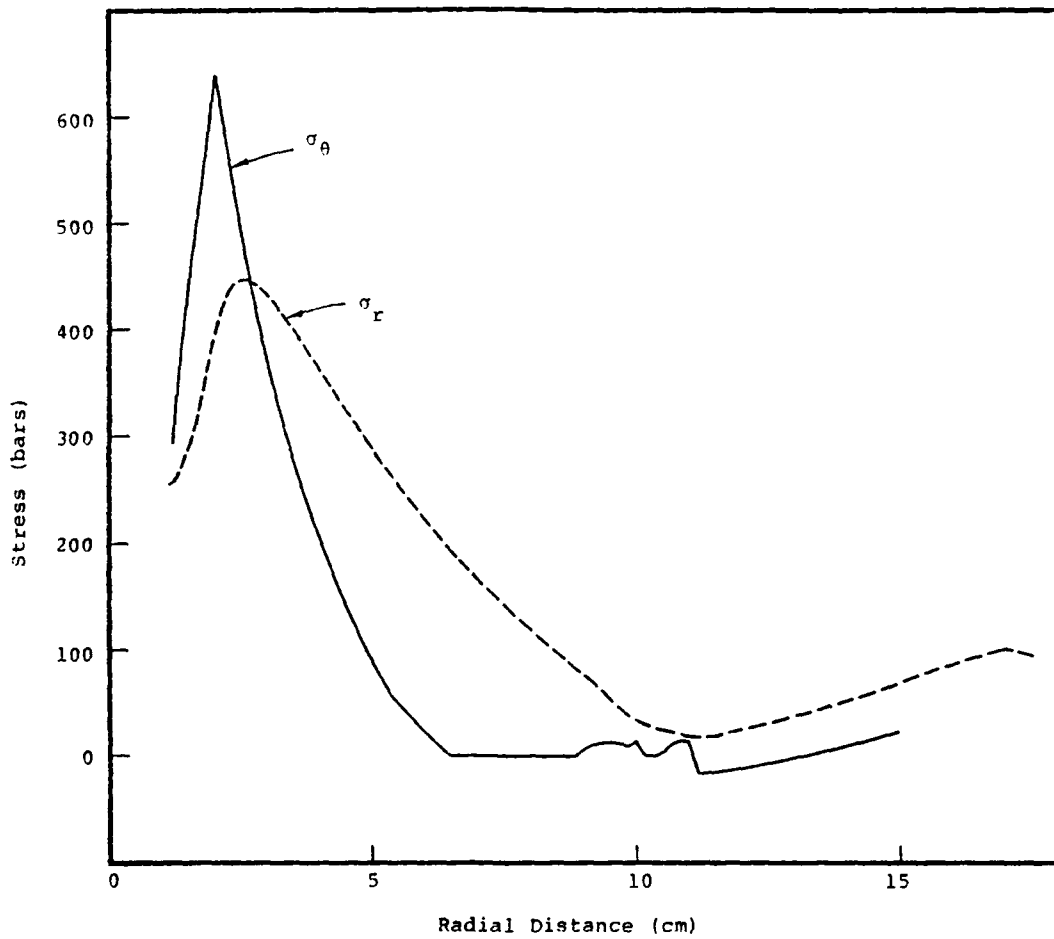


Figure 13. Residual stress fields at 84 μ sec for 2C4 calculation 1 (static failure model).

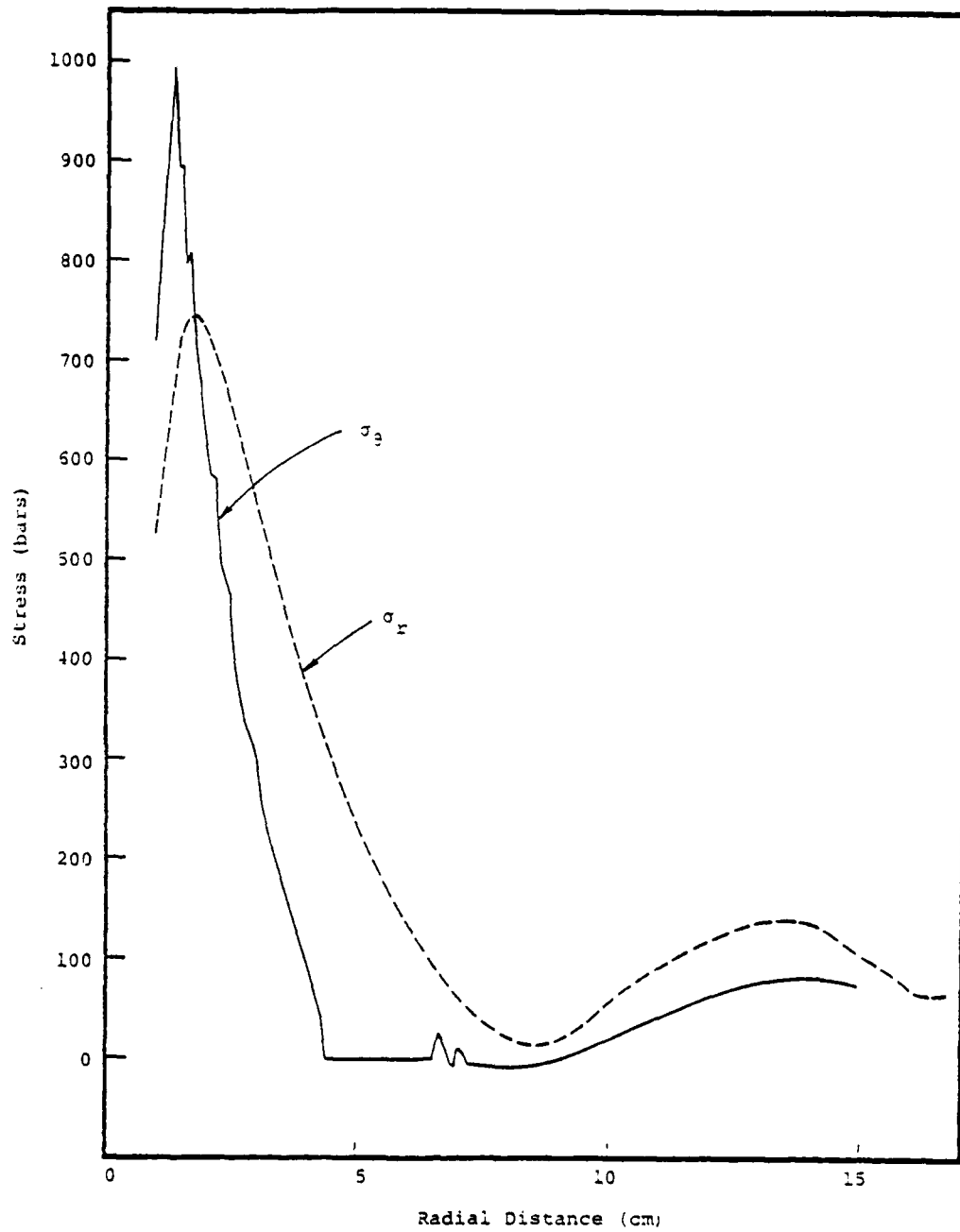


Figure 14. Residual stress fields at 79 μ sec for 2C4 calculation 7 (dynamic failure model).

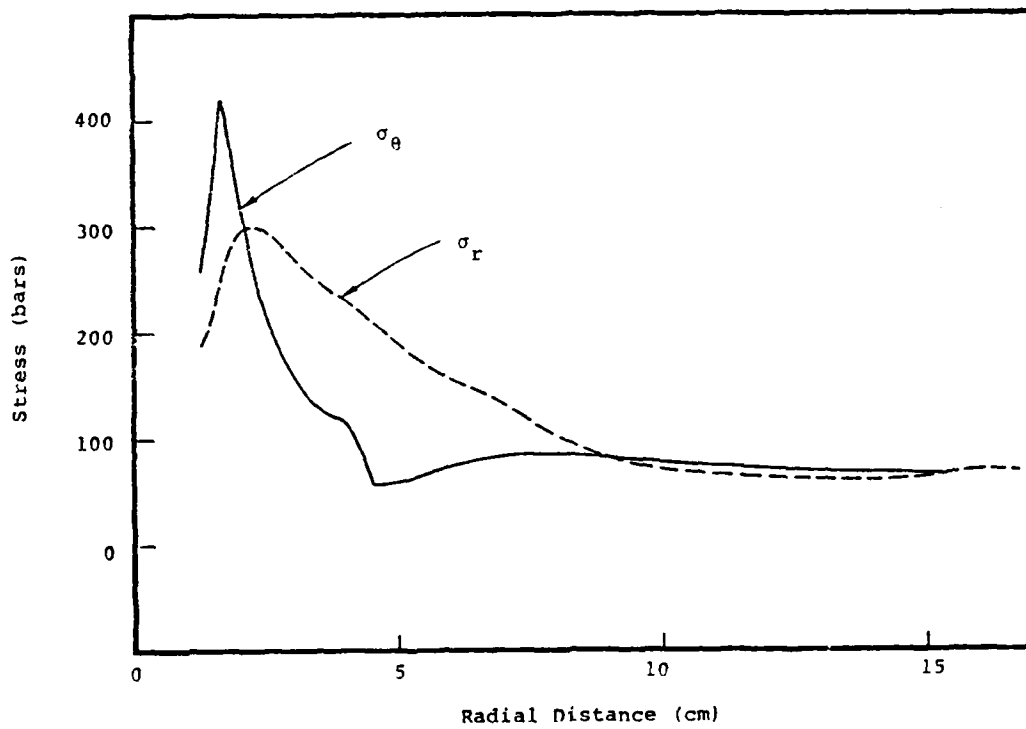


Figure 15. Residual stress fields at 124 μ sec for LD2C4 calculation 6 (static failure model).

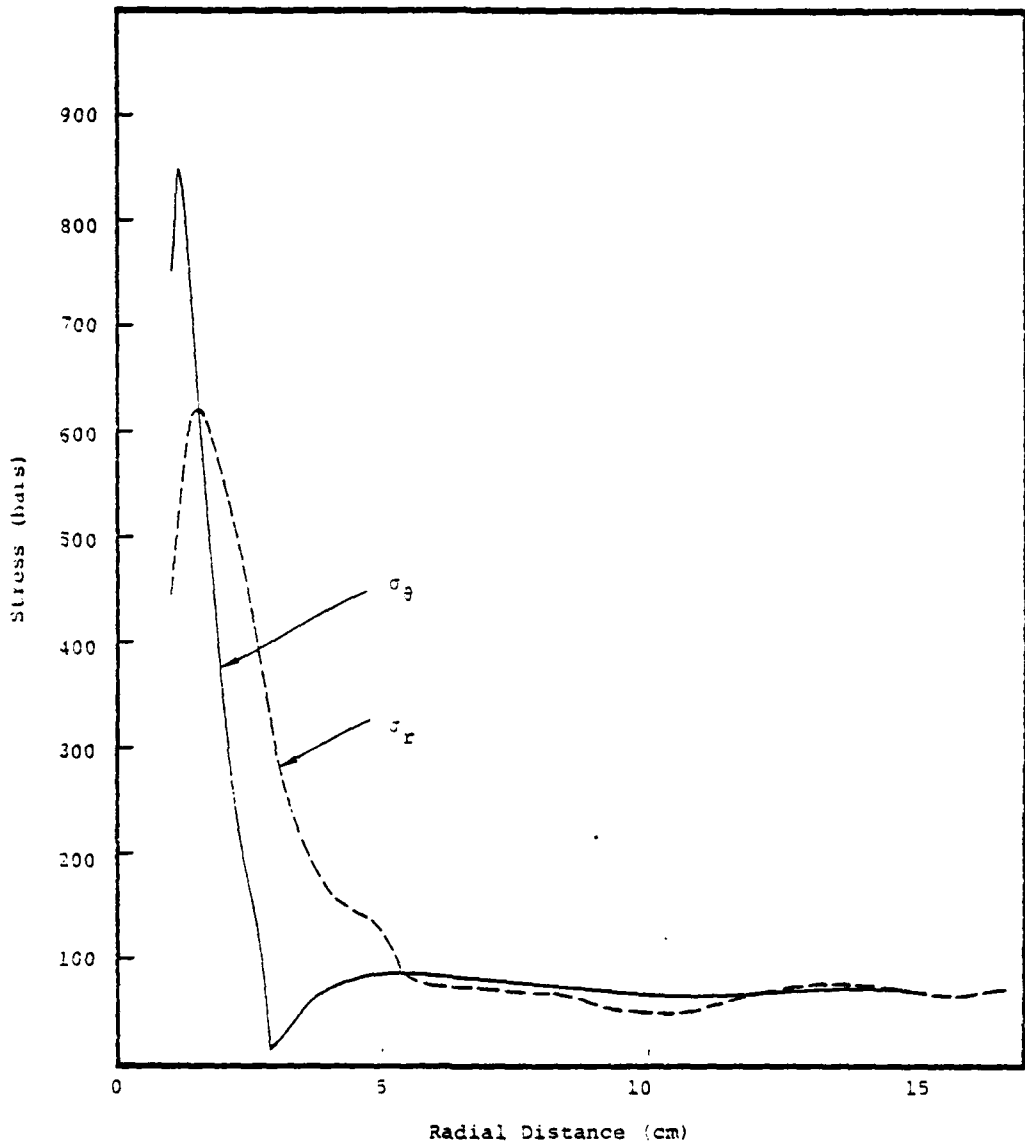


Figure 16. Residual stress fields at 110 μ sec for LD2C4 calculation 10 (dynamic failure model)

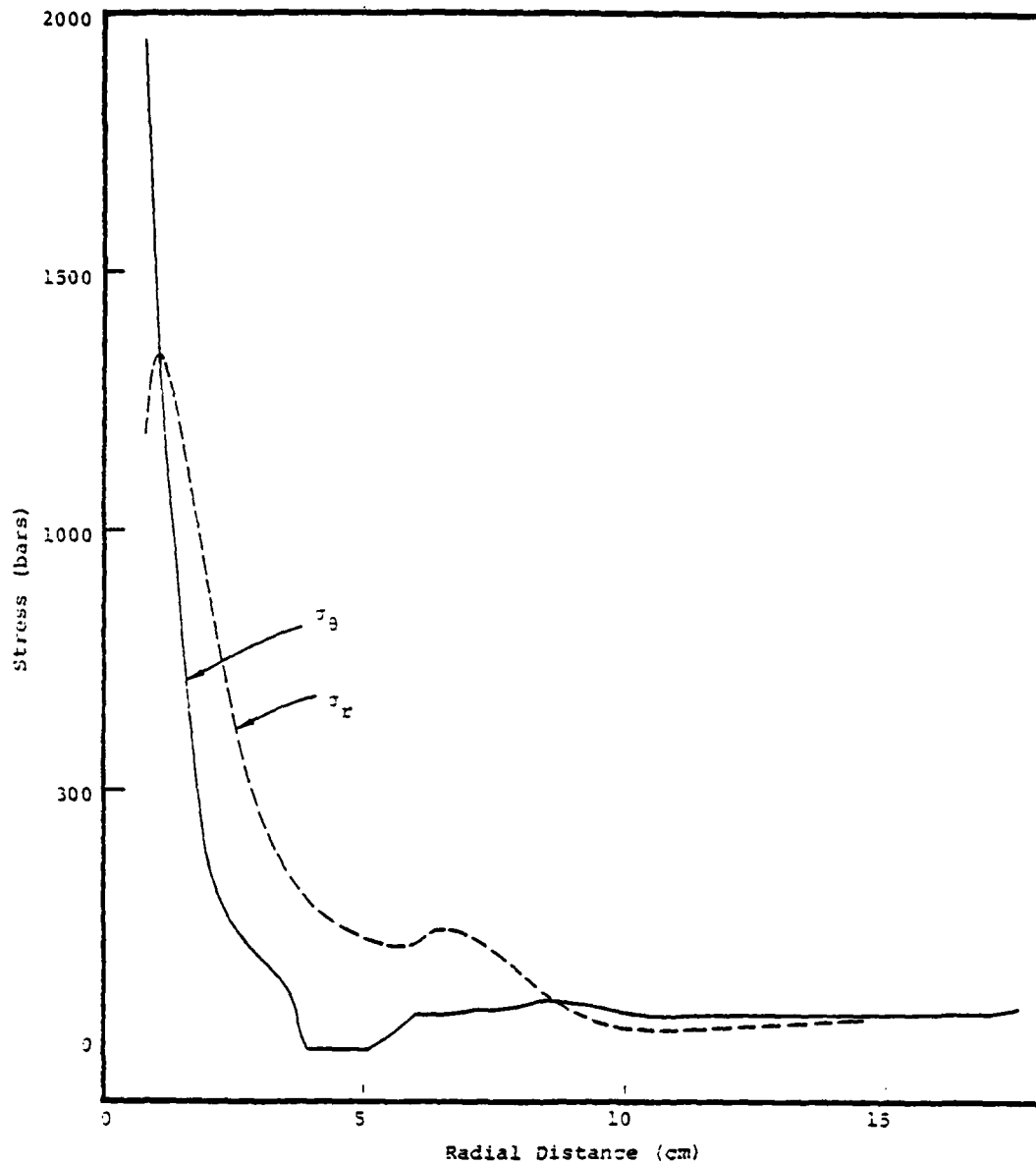


Figure 17. Residual stress fields at 95 μ sec for GS3 calculation 3 (static failure model).

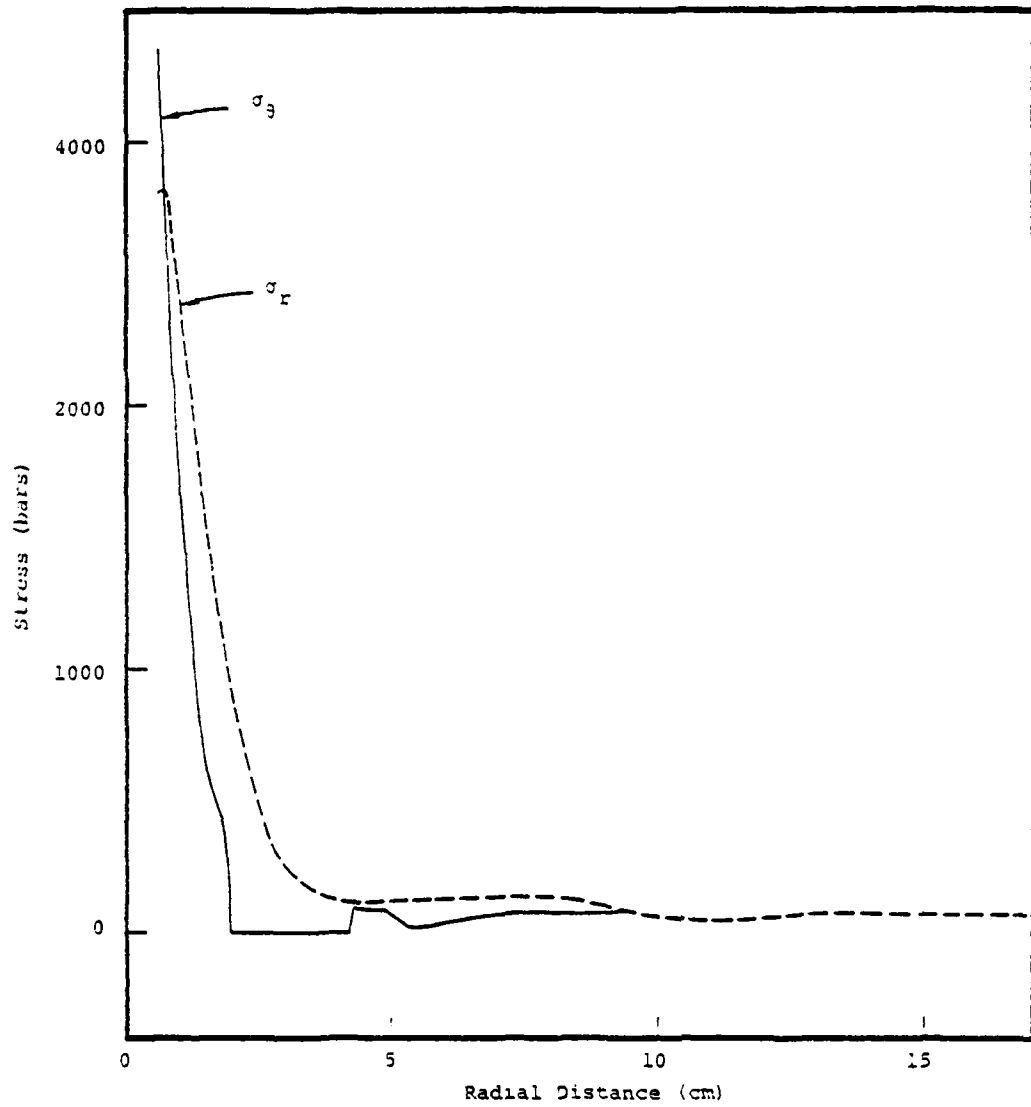


Figure 18. Residual stress fields at 74 μ sec for GS3 calculation 9 (dynamic failure model).

REFERENCES

1. Cizek, J. C. and A. L. Florence, "Laboratory Investigation of Containment in Underground Nuclear Tests", Stanford Research Institute Draft Final Report, SRI PYU-5958, submitted to DNA, January, 1978.
2. Cizek, J. C. and A. L. Florence, "Laboratory Investigation of Containment in Underground Nuclear Tests", Stanford Research Institute Draft Final Report, SRI PYU-5958, submitted to DNA, January, 1979.
3. Rimer, N., and K. Lie, "Spherically Symmetric Numerical Simulation of the SRI Grout Spheres Containment Experiments", Systems, Science and Software Topical Report SSS-R-79-3831. Submitted to DNA, October, 1978.
4. Rimer, N. and M. Friedman, "Residual Stress and Coupling from Nuclear Shots in a Cavity, Systems, Science and Software Report DNA 4591 T, April, 1978.
5. Cizek, J. C., Private Communication, August 29, 1979.
6. Cizek, J. C., Private Communication, July 16, 1979.
7. Alme, M., Private Communication, February, 1977, Air Force Weapons Laboratory Equation of State of Air Attributed to Leon Chandler, no known documentation.
8. Cizek, J. C. and A. L. Florence, "Laboratory Investigation of Stemming and Containment in Underground Nuclear Tests", Bimonthly Progress Report No. 4, September 1979.
9. Cizek, J. C., Private Communication, October 22, 1979.
10. Rimer, N., "The Relationship Between Material Properties, Residual Stresses and Cavity Radius Due to a Nuclear Explosion, Systems, Science and Software Topical Report, SSS-R-76-2907, May, 1976.

DISTRIBUTION LIST

DEPARTMENT OF DEFENSE

Defense Nuclear Agency
ATTN: SPTD, T. Kennedy
4 cy ATTN: TITL

Field Command
Defense Nuclear Agency
ATTN: FCTMD, W. Summa
ATTN: FCTK, C. Keller

Field Command Test Directorate
Defense Nuclear Agency
ATTN: FCTC, J. LaComb

Defense Technical Information Center
12 cy ATTN: DD

DEPARTMENT OF ENERGY

Department of Energy
Nevada Operations Office
ATTN: R. Newman

DEPARTMENT OF ENERGY CONTRACTORS

Lawrence Livermore National Laboratory
ATTN: D. Oakley
ATTN: B. Hudson
ATTN: B. Terhune
ATTN: J. Shearer

Los Alamos Scientific National Laboratory
ATTN: R. Brownlee
ATTN: E. Jones
ATTN: F. App
ATTN: A. Davis
ATTN: L. Germain

DEPARTMENT OF ENERGY CONTRACTORS (Continued)

Sandia National Laboratories
ATTN: C. Mehl
ATTN: C. Smith
ATTN: A. Bass

OTHER GOVERNMENT AGENCY

Department of the Interior
U.S. Geological Survey
ATTN: R. Carroll

DEPARTMENT OF DEFENSE CONTRACTORS

General Electric Company—TEMPO
ATTN: DASIAC

Pacifica Technology
ATTN: G. Kent

Physics International Co.
ATTN: E. Moore

SRI International
ATTN: A. Florence

Systems, Science & Software, Inc.
ATTN: R. Duff

Terra Tek, Inc.
ATTN: S. Green